*Metrol. Meas. Syst.*, Vol. 29 (2022) No. 3, pp. 455–468
DOI: 10.24425/mms.2022.142270

PAN POLSKA AKADEMIA NAUK

METROLOGY AND MEASUREMENT SYSTEMS
Index 330930, ISSN 0860-8229
*www.metrology.wat.edu.pl*

M&MS

# IMPLEMENTATION OF GOERTZEL-BASED FREQUENCY ESTIMATION FOR POWER QUALITY MONITORING IN EMBEDDED MEASUREMENT SYSTEMS

**Nuno M. Rodrigues[1)], Fernando M. Janeiro[2)], Pedro M. Ramos[1)]**

1) *Instituto de Telecomunicações, Instituto Superior Técnico, Universidade de Lisboa, 1049-001 Lisboa, Portugal* (*nuno.medeiros.rodrigues@tecnico.ulisboa.pt*, ✉ *pedro.m.ramos@tecnico.ulisboa.pt*, +351 218 418 485)
2) *Instituto de Telecomunicações, Universidade de Évora, 7000-671 Évora, Portugal* (*fmtj@uevora.pt*)

**Abstract**

International standards from IEC and IEEE regulate power grid parameters such as the RMS value, frequency, harmonic and interharmonic distortion, unbalance or the presence of transients, that are important to assure the quality of distributed power. Standard IEC 61000-4-30 suggests the zero crossing algorithm for the measurement of the power grid frequency, but also states that different algorithms can be used.
This paper proposes a new algorithm, the Fractional Interpolated Discrete Fourier Transform, FracIpDFT, to estimate the power grid frequency, suitable for implementation in resource limited embedded measurement systems. It is based on the non-integer Goertzel algorithm followed by interpolation at non-integer multiples of the DFT frequency resolution. The proposed algorithm is validated and its performance compared with other algorithms through numerical simulations. Implementation details of the FracIpDFT in an ARM Cortex M4 processor are presented along with frequency measurement results performed with the proposed algorithm in the developed system.

Keywords: power quality, frequency estimation, non-integer Goertzel, frequency interpolation, embedded measurement systems.



## 1. Introduction

Energy demand and environmental concerns have resulted in significant improvements in renewable energies and decentralized energy production [1]. Additionally, advances in power electronics have led to extensive use of nonlinear loads that can degrade the power grid quality [2]. The combination of these two structural changes has increased interest in *Power Quality* (PQ) research topics [3] and in distributed monitoring equipment that can be used to characterize PQ events in multiple power-grid locations [4, 5]. The main objective of these monitoring systems is to maintain the efficiency, reliability, and safety amid the integration of renewable and alternative energy sources. However, these changes represent significant costs in the electricity infrastructure [6]. Smart Grid [7] is a concept of next generation electric power



Article history: received February 18, 2022; revised May 24, 2022; accepted May 31, 2022; available online June 28, 2022.

systems that has emerged to address these concerns. Smart networks [8], *Internet of Things* (IoT) [9] and machine learning [10] aim to reshape the way power quality monitoring is addressed. Power quality monitoring is characterized by measuring the power grid harmonics, unbalances, sags, swells, and transients as defined in international standards from IEC [11, 12] and IEEE [13].

According to IEC standard 61000-4-30 [11], for class A instruments (Paragraph 5.1.1), the evaluation of the power grid frequency must be obtained every 10 s but shorter time intervals are required for specific applications. For example, in Paragraphs 3.2.3 and 3.4.1 of [12] for the evaluation of harmonics and interharmonics, a 10 cycle time span in 50 Hz power systems (200 ms) is required, and in Paragraph 4.4 of [11], the minimum time interval aggregation is also 10 cycles for 50 Hz power systems. Paragraph 5.1.1 of [11] proposes the *zero crossing* (ZC) algorithm where the fundamental frequency is obtained by dividing the number of integral cycles, counted during the considered time interval, by the cumulative duration of those cycles. To avoid false zero crossings that affect the frequency estimation, harmonics, interharmonics and noise should be attenuated using a low-pass filter.

The frequency estimation of an acquired signal is an active research topic with many contributions comparing different techniques and applications [14] including also for power quality measurements [15]. Spectral based algorithms usually start from the *Discrete Fourier Transform* (DFT) calculation, using the *Fast Fourier Transform* (FFT), followed by interpolation for frequency estimation [16–21]. Alternatively, in [22], an adaptive notch filter technique was proposed for frequency estimation by tracking the instantaneous frequency of the input signal. In [23], a time-domain model of a single-tone sinewave is used to best-fit the acquired samples in sine-fitting algorithms which estimate the signal frequency and these algorithms have been used in other areas of instrumentation and measurements [24]. Regardless of the accuracy of these algorithms, most of them have a high computational burden which makes them unsuitable for application in real-time embedded measurement systems that have limited computational abilities as well as limited storage capacities.

For the spectral based algorithms, the computation of the DFT/FFT requires considerable computational resources as well as storage capacity. One option is to use the Chirp Z [25] to estimate only spectral components near a selected range of frequencies. Alternatively, an efficient algorithm to estimate individual DFT components is the Goertzel algorithm [26] which consists on a low-pass digital filter tuned to a specific DFT frequency tone. In [27], the algorithm was adapted for application to non-integer (fractional) DFT components.

The zero crossing based algorithm suggested in [11] is suitable for implementation in resource limited devices since it consists in detecting and counting the number of zero crossings and performing two linear interpolations to refine the initial and final zero crossing instants within the time-frame. The filter used to attenuate the noise and the harmonic caused problems can be applied to each incoming sample to reduce the number of stored values. An alternative to the zero crossing algorithm must be particularly suited for implementation in embedded measurement systems and deliver some improvement over the zero crossing based algorithm.

This paper proposes a new algorithm, the *Fractional Interpolated Discrete Fourier Transform*, FracIpDFT, to estimate the power grid frequency based on the non-integer Goertzel algorithm [27] followed by an interpolation of the estimated spectral components using the *Interpolated Discrete Fourier Transform* (IpDFT) described in [16]. The proposed algorithm is compared to the ZC algorithm for the estimation of the power grid frequency nominally operating at 50 Hz for $\Delta T = 200$ ms segments (10 power grid cycles), acquired at a sampling rate of 12.5 kHz, in numerical simulations and power grid measurements.

*Metrol. Meas. Syst.*, Vol. 29 (2022), No. 3, pp. 455–468
DOI: 10.24425/mms.2022.142270

## 2. Zero crossing frequency estimation

In the IEC standard 61000-4-30 [11], Paragraph 5.1.1, the suggested algorithm for the measurement of the power grid voltage frequency is the zero crossing algorithm. To avoid multiple zero crossings caused by harmonics, interharmonics and noise, the acquired data should be filtered to reduce (ideally to eliminate) false zero crossings not caused by the voltage fundamental. The design of the digital filter is crucial to ensure computational efficiency and correct attenuation of the harmonics, interharmonics and noise. Figure 1 shows a simulated voltage signal with harmonic content and additive white noise and the filtering process, together with the ZC frequency estimation. The filter may introduce attenuation of the fundamental frequency component, but since its amplitude is not required, attenuation and even passband ripple do not affect the ZC frequency estimation.

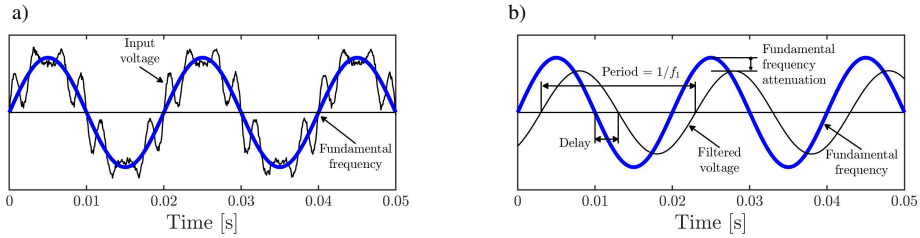


Fig. 1. Simulated example of frequency estimation using digital filtering and zero crossing detection. In (a), a simulated input voltage with a strong harmonic component and additive noise (thin line) together with the fundamental (thick blue line) are shown. In (b), the thin line corresponds to the filtered voltage and the thick line corresponds to the fundamental.

For the digital filtering, three different low-pass 6$^{\text{th}}$ order *Infinite Impulse Response* (IIR) filters were initially considered: (i) Butterworth; (ii) Chebyshev Type I and; (iii) Elliptic. The filters were designed to operate at the sampling rate of $f_s$ = 12.5 kHz, with a 60 Hz passband, 3 dB maximum attenuation within the passband and, for the elliptic filter, at least 100 dB attenuation in the stopband. The obtained amplitude response of the three filters is represented in Fig. 2. The relative attenuation from the 2$^{\text{nd}}$ to 5$^{\text{th}}$ harmonics as a function of the fundamental frequency, $f_1$, within the [40; 60] Hz frequency range is also shown. The elliptic filter presents higher relative attenuation (particularly for the 3$^{\text{rd}}$ harmonic) and was therefore the filter selected to be used for frequency estimation using zero crossing detection. Note that, in some situations, a band pass filter might be a better solution due to the presence of subharmonics. However, the implementation of such filter might require more computational power due to its higher order to maintain the 100 dB attenuation in the stopband.

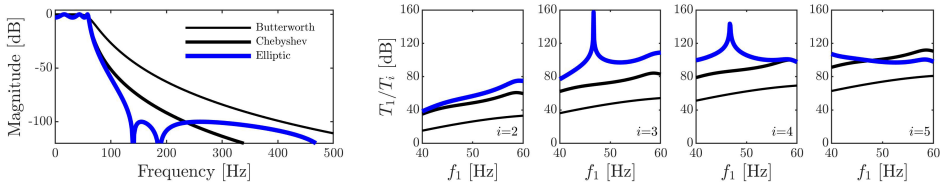


Fig. 2. The left plot represents the magnitude response of the three different low-pass 6$^{\text{th}}$ order IIR considered filters: Butterworth, Chebyshev Type I and Elliptic. The remaining plots depict the relative attenuation of the 2$^{\text{nd}}$, 3$^{\text{rd}}$, 4$^{\text{th}}$ and 5$^{\text{th}}$ harmonics as a function of the voltage fundamental frequency, $f_1$.

## 3. Fractional Interpolated Discrete Fourier Transform (FracIpDFT)

This section describes the proposed algorithm for frequency estimation of a power grid voltage waveform, the *Fractional Interpolated Fourier Transform* (FracIpDFT). A single-tone voltage is represented by

$$x(t) = A\cos(2\pi f_1 t + \phi), \tag{1}$$

where $f_1$ is the fundamental frequency, $A$ is the amplitude (without loss of generality, in the simulations $A = 1$ V is used) and $\phi$ is the initial phase. Acquiring $N$ samples at a sampling frequency $f_s$, results in a DFT frequency resolution of $\Delta f = 1/\Delta T = f_s/N$. The DTFT of $x(t)$ is

$$X(\Omega) = \frac{A}{2}\left[W_R(\Omega - \Omega_1)e^{j\phi} + W_R(\Omega + \Omega_1)e^{-j\phi}\right], \tag{2}$$

where $\Omega = 2\pi f/f_s$ is the normalized angular frequency, $\Omega_1 = 2\pi f_1/f_s$ represents the normalized fundamental angular frequency of $x(t)$ and $W_R(\Omega)$ is the rectangular window spectral response given by

$$W_R(\Omega) = \frac{\sin(\Omega N/2)}{\sin(\Omega/2)} e^{-j\frac{\Omega}{2}(N-1)}. \tag{3}$$

Figure 3 shows the amplitude spectra of a simulated voltage $x(t)$ with $f_1 = 51$ Hz and $\Delta f = 1/\Delta T = 1/0.2 = 5$ Hz. Since the frequency does not correspond to an integer multiple of the DFT spectral resolution, $\Delta f$, there is spectral leakage, and the frequency must be estimated through interpolation.

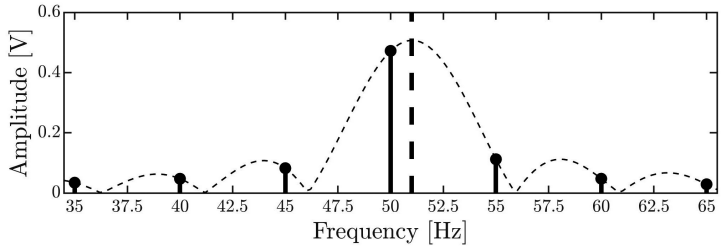


Fig. 3. Simulated DTFT amplitude for a 51 Hz sine voltage with spectral leakage (thin dashed line). The vertical dashed line represents the voltage frequency, and the bins represent the DFT spectral amplitudes for $\Delta f = 5$ Hz.

Although the FFT can be applied to obtain all the voltage spectrum bins with $\Delta f$ resolution, the Goertzel algorithm [26] is an efficient process to compute a single DFT component without calculating the FFT. The Goertzel calculation of the DFT $k$-th spectral component consists of two consecutive independent steps: (i) application of a 2$^{\text{nd}}$ order IIR filter with real coefficients and; (ii) estimation of the Goertzel DFT $k$-th component using only the last two outputs of the IIR filter from step (i). The difference equation of the IIR filter for the first step is

$$s[n] = x[n] + 2\cos\left(\frac{2\pi k}{N}\right)s[n-1] - s[n-2], \tag{4}$$

where $x[1,\ldots,N]$ are the acquired samples and $s[1,\ldots,N]$ are the filter outputs with $s[0] = s[-1] = 0$. The Goertzel algorithm was generalized for non-integer multiples $k$ of the DFT

*Metrol. Meas. Syst.*, Vol. 29 (2022), No. 3, pp. 455–468
DOI: 10.24425/mms.2022.142270

frequency resolution [27], allowing the computation of the spectrum coefficients at any desired frequency and, in this case, the second step is

$$y_k[N] = \left(s[N] - e^{-j\frac{2\pi k}{N}} s[N-1]\right) e^{-j2\pi k}. \tag{5}$$

Figure 4 shows an example of the amplitude and phase of the spectrum of a sine voltage with $f_1 = 51$ Hz sampled at $f_s = 12.5$ kHz with $\Delta f = 5$ Hz. The vertical lines represent the frequency components, computed by the non-integer Goertzel algorithm with 1 Hz resolution, while the dashed line represents (2).

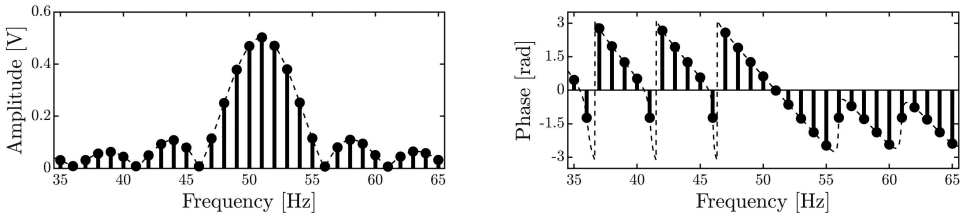


Fig. 4. Simulated spectrum for a $f_1 = 51$ Hz voltage signal with spectral leakage. The dashed line represents the DTFT of the voltage sampled with $\Delta f = 5$ Hz and the vertical bins show the spectral coefficients computed by the Goertzel algorithm with 1 Hz resolution.

For the computation of $s[n]$, only three values of (4) need to be stored in memory ($s[n]$, $s[n-1]$ and $s[n-2]$) and (5) is only used once to obtain $y_k[N]$ from $s[N]$ and $s[N-1]$ through two complex multiplications. Since $k$ and $N$ are known, the terms $e^{-j2\pi k/N}$, $e^{-j2\pi k}$ and $\cos(2\pi k/N)$ can be calculated beforehand and stored to further improve the algorithm computational performance. The complex exponentials in (5) are used at the end of the Goertzel algorithm (in this paper, every $\Delta T = 200$ ms), while the calculation of $s[n]$, performed for each sample using (4), only involves real numbers. As shown in [27], when $N$ is a power of two, corresponding to a faster optimized FFT, the calculation of $K$ Goertzel components is better than the full FFT as long as $K < \min[4N/7; 2\log_2(N)]$, where the first term corresponds to the memory size and the second accounts for the number of operations involved (as described in [27], if $N$ is a power of 2, the FFT requires $6N\log_2(N)$ real operations whereas each Goertzel algorithm requires $3N$). For $N > 12$, the second term is dominant and thus, the Goertzel requires less memory and fewer operations when $K < 2\log_2(N)$. When the number of samples is not a power of two, the FFT requires more operations and thus the Goertzel advantage is even more significant.

A commonly used strategy to estimate the frequency of an acquired waveform with spectral leakage is to interpolate the relevant spectral components. Renders *et al.* [16] derived analytical expressions for the two point interpolation, when a rectangular window is considered, which is the IpDFT algorithm used in this paper. Multipoint interpolation and the use of windows has also been studied in the literature, such as the Hann window multipoint interpolation [17].

The FFT+IpDFT [16] starts by identifying the two DFT bins, $f_A$ and $f_B$, with $f_B > f_A$, where one is the largest amplitude component and the other is its largest neighbour to minimize the relative influence that noise can have on the used neighbour component (in the example of Fig. 3, $f_A = 50$ Hz, $f_B = 55$ Hz). The complex DFT coefficients for these bins are $S_A = U_A + jV_A$ and $S_B = U_B + jV_B$, and the interpolated estimated frequency is

$$\hat{f}_1 = \frac{f_s}{2\pi} \arccos\left[\frac{Z_B\cos(\Omega_B) - Z_A\cos(\Omega_A)}{Z_B - Z_A}\right], \tag{6}$$

where $\Omega_A = 2\pi f_A/f_s$, $\Omega_B = 2\pi f_B/f_s$ and

$$\begin{aligned} Z_A &= V_A \frac{K_{\text{opt}} - \cos(\Omega_A)}{\sin(\Omega_A)} + U_A \,, \\ Z_B &= V_B \frac{K_{\text{opt}} - \cos(\Omega_B)}{\sin(\Omega_B)} + U_B \,, \\ K_{\text{opt}} &= \frac{(V_B - V_A)\sin(\Omega_A) + (U_B - U_A)\cos(\Omega_A)}{U_B - U_A} \,. \end{aligned} \tag{7}$$

The uncertainty of the FFT+IpDFT [16] frequency estimate depends on the amount of noise in the acquired voltage. In particular, when the spectral leakage is very reduced, the neighbour components have a very low amplitude and the selection of the highest amplitude neighbour is significantly affected by the noise contributions at those DFT components, resulting in increased frequency uncertainty when compared with situations where there is significant spectral leakage. Reducing the DFT frequency resolution, $\Delta f$, leads to spectral bins that are closer to each other which reduces the noise influence, but this requires longer acquisition segments and the interpolation algorithm is still significantly worse in reduced spectral leakage situations. Another possibility is computing the complex coefficients at non-integer multiples of the frequency resolution, which can be done with non-integer Goertzel filters. Although (6) and (7) were derived considering that $f_A$ and $f_B$ are located at integer multiples of $\Delta f$, they are also valid if the frequency bins used for the interpolation are integer multiples of $\Delta f/2$ as long as the frequency spacing between the components used for interpolation remains at $\Delta f$ (*i.e.*, $f_B - f_A = \Delta f$).

The proposed FracIpDFT algorithm for frequency estimation consists in computing the Goertzel components spaced at $\Delta f/2$ within the frequency range of interest and choosing two $\Delta f$ spaced spectral components to perform the interpolation using the IpDFT (6)–(7). To illustrate the choice of the components for interpolation, Fig. 5 shows the situation presented in Fig. 3 with computed spectral components at integer multiples of $\Delta f/2$. In this case, the highest amplitude component is located at 50 Hz which, in [16], would be used with the 55 Hz component for interpolation. However, selecting the components at 47.5 Hz and 52.5 Hz would lead to a better frequency estimation due to its higher aggregated amplitude, thus reducing the effect of noise. Therefore, in the proposed algorithm, after the non-integer Goertzel components are calculated, the highest amplitude is detected and the interpolation is performed with its two neighbour components. Since the power grid measurement frequency range is [42.5; 57.5] Hz (Paragraph 5.1.2 of [11]), to implement the proposed algorithm, nine Goertzel filters (located from 40 Hz up to 60 Hz with 2.5 Hz spacing) are needed to cover this frequency range.

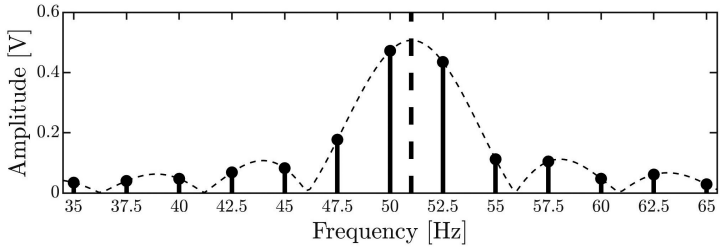


Fig. 5. Simulated example of the amplitude spectra for a 51 Hz sine voltage with spectral leakage (thin dashed line). The vertical dashed line represents the actual voltage frequency and the bins represent the spectral amplitudes at integer multiples of $\Delta f/2$, with $\Delta f = 5$ Hz.

*Metrol. Meas. Syst.*, Vol. 29 (2022), No. 3, pp. 455–468
DOI: 10.24425/mms.2022.142270

## 4. Simulation results

In this section, a comparison between the proposed FracIpDFT algorithm and other frequency estimation algorithms is presented. The results correspond to simulations using a 12.5 kHz sampling rate and 200 ms segments, corresponding to $N = 2500$ samples per segment. The Cramér–Rao Lower Bound (*CRLB*) for the frequency estimation of digitally acquired signals when the phase is unknown, is given by (3.41) of [28]

$$CRLB = \frac{f_s}{2\pi}\sqrt{\frac{12}{N\left(N^2-1\right)SNR}}, \tag{8}$$

where *SNR* is the signal to noise ratio.

Figure 6 presents the frequency estimation *RMSE* (Root Mean Square Error) relative to the *CRLB* simulation results obtained with three different Hann window interpolations (2, 3 and 5 point interpolation) [17], the ZC algorithm, FFT+IpDFT (described in [16]), sine-fitting and the proposed FracIpDFT algorithm, considering additive white noise with *SNR* = 13.98 dB. The sine-fitting algorithm is included only for the purpose of comparison since its implementation complexity makes it unsuitable for embedded system real-time operation. The results, obtained by $10^5$ random noise and phase realizations, show that the sine-fitting algorithm is the best frequency estimator with a relative *RMSE* close to 1 for the entire tested frequency range. The second best option is the proposed FracIpDFT algorithm, where the worst relative result is around 1.2 for frequencies at the midpoints of the Goertzel filters locations (*i.e.*, $f_1 = m\Delta f \pm \Delta f/4$ with $m \in \mathbb{N}$).

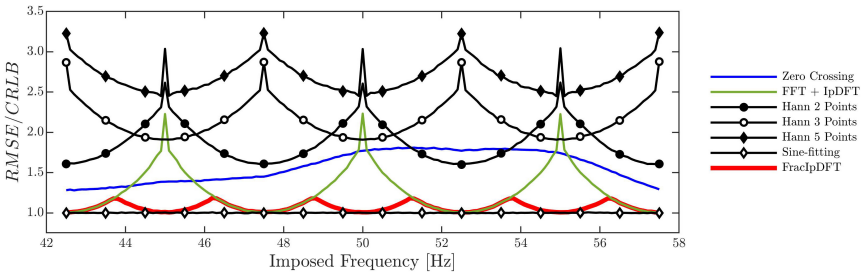


Fig. 6. Frequency estimation *RMSE* relative to the *CRLB* obtained by simulation for different *RMSE* and *CRLB* estimation algorithms including additive noise with *SNR* = 13.98 dB. Simulation results were obtained from $10^5$ random noise and random initial phase realizations and a 0.1 Hz step.

Since the multipoint Hann window algorithms are significantly worse than the other considered algorithms, these algorithms are discarded from the following analysis. Figure 7 shows the *RMSE* of the estimated frequency as a function of the *SNR* for two different frequencies corresponding to the best (Fig. 7a with $f_1 = 50$ Hz) and worst (Fig. 7b with $f_1 = 51.25$ Hz) frequency estimation by the proposed FracIpDFT algorithm.

In Fig. 7a the voltage frequency is 50 Hz corresponding to one of the computed Goertzel filters and the FracIpDFT algorithm uses the components at 47.5 Hz and 52.5 Hz for interpolation. In this case, the frequency estimation is as good as the estimation of the sine-fitting algorithm and approaches the *CRLB* for the considered *SNR* range. The FFT+IpDFT algorithm presents the worst *RMSE* because there is no spectral leakage (the algorithm performs worse due to the relative noise influence on the selection of highest amplitude neighbour), while the standard ZC algorithm also has a considerable *RMSE* when compared with the *CRLB*. The results presented

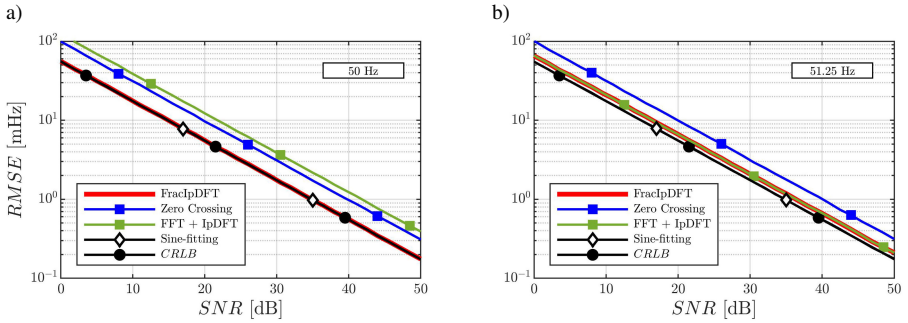


Fig. 7. Frequency estimation *RMSE* obtained by simulation for different algorithms as a function of *SNR* for two frequency values: a) 50 Hz; b) 51.25 Hz. Simulation results were obtained from $10^5$ random noise and random initial phase realizations.

in Fig. 7b correspond to a frequency of 51.25 Hz, which is one of the midpoints between two computed Goertzel filters. The *RMSE* of the proposed FracIpDFT algorithm is equal to the *RMSE* of the FFT+IpDFT algorithm but better than the ZC algorithm – the ZC achieves relative *RMSE* values between 1.8 and 1.9, while both the FFT+IpDFT and the proposed FracIpDFT algorithms present results around 1.2. For the range of frequencies and *SNR* considered, with the exception of the sine-fitting, the proposed FracIpDFT algorithm presents the best *RMSE*.

Harmonics and interharmonics are PQ events that can influence the nominal frequency estimation. To study that influence, even in the presence of spectral leakage, two fundamental frequencies were used: 50 Hz (where the proposed method has better performance) and 51.25 Hz (where the proposed method has a higher *RMSE*). For this test the influence of an interfering component in the range 60 Hz to 160 Hz for the two different fundamental frequencies was used and the results are presented in Fig. 8. The interfering component amplitude is 5 % of the fundamental which is higher than the compatibility level for the interharmonic voltage defined in IEC 61000-2-2 [29]. Overall, the presented method is better than the zero crossing and the 3 point Hann method (the

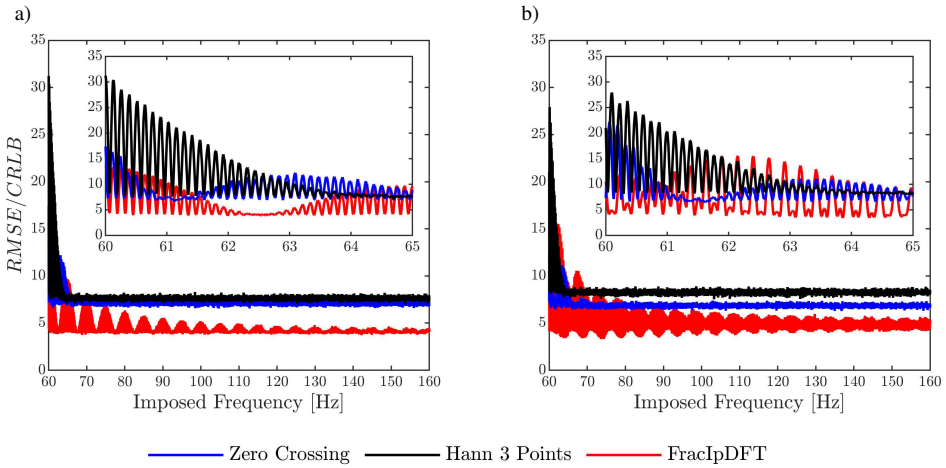


Fig. 8. Harmonics and interharmonics test with the influence of an interfering component in the 60 Hz to 160 Hz range with a 0.1 Hz step. Two fundamental frequencies were used: 50 Hz (a) and 51.25 Hz (b).

*Metrol. Meas. Syst.*, Vol. 29 (2022), No. 3, pp. 455–468
DOI: 10.24425/mms.2022.142270

best of the three Hann methods). The insets in Fig. 8 show that for some interfering frequencies the zero crossing and 3 point Hann algorithms can slightly outperform the proposed method. However, in general the proposed algorithm performs better.

## 5. Implementation and measurement results

The proposed FracIpDFT algorithm is implemented in an STM 32F411EDISCOVERY development kit. The microcontroller (STM32F411VE) is an ARM 32-bit Cortex-M4 working at 100 MHz with the internal 12-bit ADC configured to continuously acquire samples using interrupts to trigger the sampling and conversion. In Fig. 9 two flowcharts of the implementation in the embedded measurement system are presented.

The main flowchart, Fig. 9a, includes the configuration of the ADC, the configuration of the interrupts that retrieves each sample according to the sampling rate and, when 2 500 samples are completed (corresponding to a 10 cycle segment of the nominal power grid frequency at the 12.5 kHz sampling rate), estimates the power grid frequency. The flowchart represented in Fig. 9b

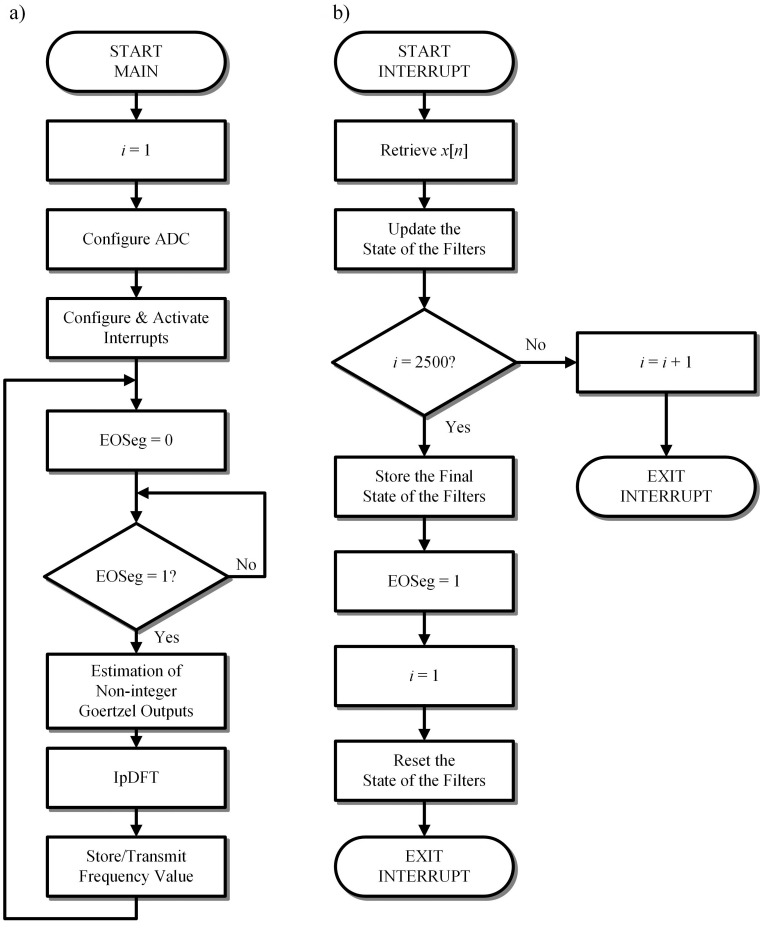


Fig. 9. Main flowchart (a) of the embedded frequency measurement system and interrupt flowchart (b).

corresponds to the interrupt routine executed as each new sample arrives. The sample value is applied to the nine Goertzel filters to update their states according to (4). When the number of samples reaches 2 500, the segment has ended, and the states of the filters are stored and reset to start processing the next segment. An end of segment flag, EOSeg, is set to 1 so that the main program can perform the final calculations to estimate the frequency. In the main program, when the EOSeg flag is detected as 1, the outputs of the Goertzel filters are estimated using the stored final states and (5). From these, two components are selected for the IpDFT according to the procedure described in Section 3. The IpDFT is then applied to estimate the frequency with these two components using (6) and (7). The final frequency estimation steps require less than 1 ms and during this process, new samples are being acquired and processed by the Goertzel filters.

To test the capabilities of the proposed embedded system an Agilent 33250A function generator was used to produce a sinewave voltage. For this test, the Agilent 33250A output includes a DC component since the STM ADC input is unipolar. Figure 10 presents the frequency estimation histograms obtained with the embedded measurement device and the FracIpDFT proposed algorithm for 50 Hz and 51.25 Hz. The expanded uncertainty, obtained with a 1.96 coverage factor, is 0.28 mHz for 50 Hz and 0.40 mHz for 51.25 Hz.

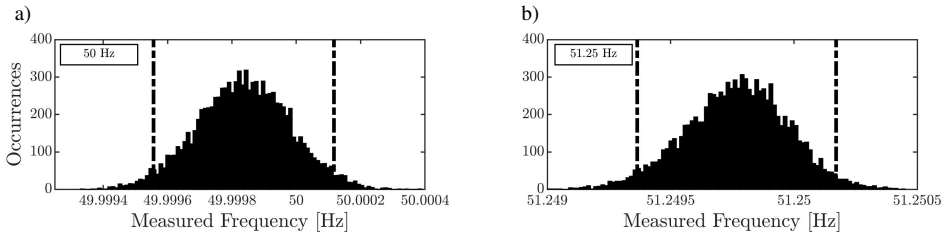


Fig. 10. Histograms of $10^4$ FracIpDFT frequency estimations using a function generator to impose the 50 Hz (a) and 51.25 Hz (b) frequencies. The thick dash-dot lines correspond to the 95 % confidence interval limits obtained with a 1.96 coverage factor ([49.999 56; 50.000 12] Hz and [51.249 36; 51.250 17] Hz).

To validate the proposed FracIpDFT frequency estimation algorithm, zero crossing was also implemented in the same development kit to perform direct comparisons between the two algorithms using the same real power grid data. In addition, an Agilent 53131A universal counter was used to measure the power grid frequency so that the results can be compared with the proposed FracIpDFT results. Since the frequency estimation is performed every 200 ms, the 53131A is configured to measure the frequency with a 200 ms gate time. The interface with the power grid is made with an analog conditioning circuit that includes a voltage divider, to reduce the power grid voltage amplitude, and the addition of a DC component. The voltage divider can be replaced with a Hall Effect sensor to isolate the electrical power grid from the STM. Figure 11a shows two periods (40 ms) of a real electrical voltage grid signal acquired at 12.5 kHz. As shown in Fig. 11b, which corresponds to a 10 s acquisition, the signal has a significant harmonic content, which results in a –35.64 dB THD.

Figure 12 presents the results of 48 hours continuous measurements with the embedded system implemented algorithms: (a) FracIpDFT measurements; and (b) the difference between the FracIpDFT and zero crossing algorithms, which never exceeds 10 mHz (0.02 %). The system can measure continuously for an unlimited amount of time because the samples are processed and discarded and the measurement results are, in this case, not locally stored.

The results shown in Fig. 13 correspond to the estimated frequency of the electrical power grid over a 60 minute time span of the proposed FracIpDFT and Agilent 53131A universal

*Metrol. Meas. Syst.*, Vol. 29 (2022), No. 3, pp. 455–468
DOI: 10.24425/mms.2022.142270

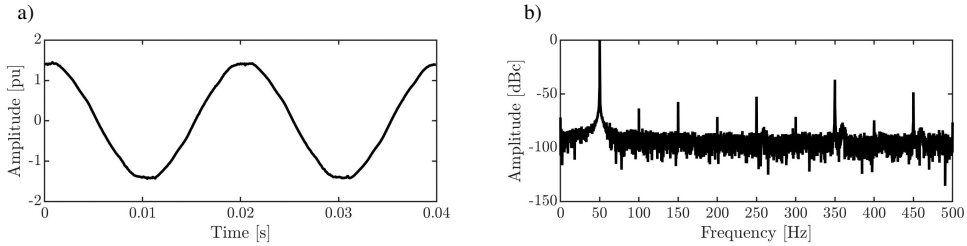


Fig. 11. Real electrical power grid voltage time representation (a) and spectrum (b). The THD is –35.64 dB for a 10 s segment with a 12.5 kHz sampling rate.

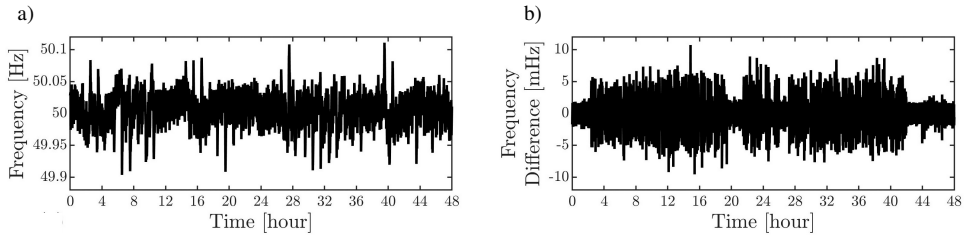


Fig. 12. Estimated power grid frequency during 48 hours using the embedded measurement system with FracIpDFT (a). ZC was used for comparison and the difference between the results obtained with both algorithms, represented in (b), is below 10 mHz.

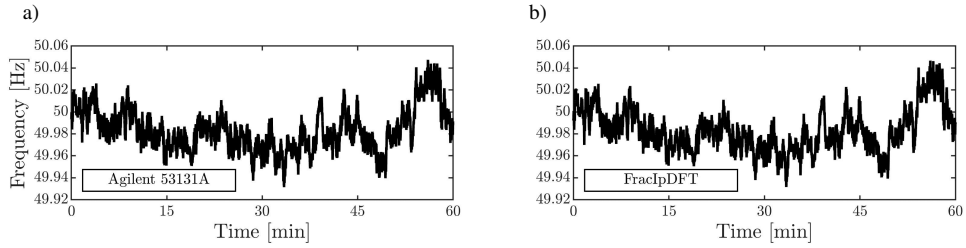


Fig. 13. Electrical power grid frequency estimation over a 60 minute time span: (a) results from the Agilent 53131A universal counter/timer with a gate time of 200 ms; and (b) frequency estimation obtained with the implemented embedded measurement system using the proposed FracIpDFT algorithm.

counter measurements. The results highlight that the proposed embedded device and algorithm tracks the frequency variations and the results are similar to those obtained with the 53131A. A direct comparison of the results cannot be performed because the measurements cannot be synchronized.

## 6. Conclusions

In this paper a new algorithm, FracIpDFT, is proposed to estimate the power grid frequency using a limited number of Goertzel filters and spectral interpolation. The algorithm is based on the Goertzel algorithm implemented as second-order IIR filters making it suitable for implementation in resource limited embedded measurement systems.

The FFT+IpDFT results are close to the *CRLB* with significant spectral leakage but worsen when spectral leakage is reduced because of increased relative noise influence on the lower amplitude neighbour. In the proposed FracIpDFT, the Goertzel filters are at the frequencies of the FFT spectral components ($m\Delta f$) and additional filters are centered in the middle of the FFT spectral components ($m\Delta f + \Delta f/2$) so that, when spectral leakage is reduced, the selected interpolation components are the intermediate components to avoid the influence of noise in the lower amplitude components. The performance of the proposed algorithm is compared with the performance of other algorithms such as zero crossing, sine-fitting and multipoint Hann window algorithms and the results are presented in Fig. 6. The noise sensitivity analysis, Fig. 7, has shown that additive white noise has a lower influence on the proposed FracIpDFT algorithm when compared with the ZC algorithm.

Details of the proposed FracIpDFT algorithm implementation in a low-cost embedded development kit were presented. To assess the frequency estimation capabilities of the FracIpDFT, an analysis was performed for a generated sinewave and the results, Fig. 10, show a 95 % confidence interval of [49.999 56; 50.000 12] Hz for 50 Hz and [51.249 36; 51.250 17] Hz for 51.25 Hz. Side by side implementation of the proposed FracIpDFT and the ZC algorithms in the embedded measurement system yielded the results presented in Fig. 12 which demonstrate the capability of the proposed algorithm to continuously monitor the power grid frequency with results similar to those obtained with the zero crossing algorithm. The results obtained over a 60 minute time span (Fig. 13) with the proposed FracIpDFT algorithm and with the Agilent 53131A show that the algorithm can successfully track the power grid frequency variations. Overall, the proposed FracIpDFT algorithm has a similar implementation complexity and memory requirements as the zero crossing algorithm but produces better results, and thus it is a good option for embedded system implementation.

**Acknowledgements**

This work was developed under the PhD program of the Fundação para a Ciência e a Tecnologia (FCT) reference SFRH/BD/130327/2017 and is funded by FCT/MCTES through national funds and, when applicable, co-funded EU funds under the project UIDB/EEA/50008/2020.

**References**

[1] Sorrell, S. (2015). Reducing energy demand: A review of issues, challenges and approaches. *Renewable and Sustainable Energy Reviews*, *47*, 74–82. https://doi.org/10.1016/j.rser.2015.03.002

[2] Liang, X. (2017). Emerging power quality challenges due to integration of renewable energy sources. *IEEE Transactions on Industry Applications*, *53*(2), 855–866. https://doi.org/10.1109/TIA.2016.2626253

[3] Montoya, F. G., Cruz, A. G., Montoya, M. G., & Agugliaro, F. M. (2016). Power quality techniques research worldwide. A review. *Renewable and Sustainable Energy Reviews*, *54*(2), 846–856. https://doi.org/10.1016/j.rser.2015.10.091

[4] Parle, J. A., Madrigal, M., & Acha, E. (2001). Trends in power quality monitoring. *IEEE Power Engineering Review*, *21*(10), 3–21. https://doi.org/10.1109/39.954584

[5] Radil, T., Ramos, P. M., Janeiro, F. M., & Serra, A. C. (2008). PQ monitoring system for real-time detection and classification of disturbances in a single-phase power system. *IEEE Transactions on Instrumentation and Measurement*, *57*(8), 1725–1733. https://doi.org/10.1109/TIM.2008.925345

*Metrol. Meas. Syst.*, Vol. 29 (2022), No. 3, pp. 455–468
DOI: 10.24425/mms.2022.142270

[6] Yang, Y., Divan, D. M., Harley, R. G., & Habetler, T. G. (2006). Power line sensornet – A new concept for power grid monitoring. *IEEE Power Engineering Society General Meeting*. https://doi.org/10.1109/PES.2006.1709566

[7] Muscas, C., Pau, M., Pegoraro, P. A., & Sulis, S. (2015). Smart electric energy measurements in power distribution grids. *IEEE Instrumentation & Measurement Magazine*, *18*(1), 17–21. https://doi.org/10.1109/MIM.2015.7016676

[8] Velazquez, L. M., Troncoso, R. R., Ruiz, G. H., Sotelo, D. M., & Rios, R. O. (2017). Smart sensor network for power quality monitoring in electrical installations. *Measurement*, *103*, 133–142. https://doi.org/10.1016/j.measurement.2017.02.032

[9] Alavi, A. H., Jiao, P., Buttlar, W. G., & Lajnef, N. (2018). Internet of Things-enabled smart cities: State-of-the-art and future trends. *Measurement*, *129*, 589–606. https://doi.org/10.1016/j.measurement.2018.07.067

[10] Ribeiro, E. G., Mendes, T. M., Dias, G. L., Faria, E. R. S., Viana, F. M., Barbosa, B. H. G., & Ferreira, D. D. (2018). Real-time system for automatic detection and classification of single and multiple power quality disturbances. *Measurement*, *128*, 276–283. https://doi.org/10.1016/j.measurement.2018.06.059

[11] IEC 61000-4-30 (2015). Electromagnetic compatibility (EMC) – part 4–30: Testing and measurement techniques – Power quality measurement methods, Edition 3.0

[12] IEC 61000-4-7 (2009). Electromagnetic compatibility (EMC) – part 4–7: Testing and measurement techniques – General guide on harmonics and interharmonics measurements and instrumentation, for power supply systems and equipment connected thereto, Edition 2.1

[13] IEEE Std 1159-2009 (2009). IEEE Recommended Practice for Monitoring Electric Power Quality. https://doi.org/10.1109/IEEESTD.2009.5154067

[14] Slepička, D., Agrež, D., Lapuh, R., Nunzi, E., Petri, D., Radil, T., Schoukens, J., & Sedláček, M. (2010, May). Comparison of nonparametric frequency estimators. In 2010 IEEE Instrumentation & Measurement Technology Conference Proceedings (pp. 73-77). IEEE. https://doi.org/10.1109/IMTC.2010.5488181

[15] Ramos, P. M., & Serra, A. C. (2009). Comparison of frequency estimation algorithms for power quality assessment. *Measurement*, *42*(9), 1312–1317. https://doi.org/10.1016/j.measurement.2008.04.013

[16] Renders, H., Schoukens, J., & Vilain, G. (1984). High-accuracy spectrum analysis of sampled discrete frequency signals by analytical leakage compensation. *IEEE Transactions on Instrumentation and Measurement*, *33*(4), 287–292. https://doi.org/10.1109/TIM.1984.4315226

[17] Agrež, D. (2007). Dynamics of frequency estimation in the frequency domain. *IEEE Transactions on Instrumentation and Measurement*, *56*(6), 2111–2118. https://doi.org/10.1109/TIM.2007.908240

[18] Belega, D., Petri, D., & Dallet, D. (2014). Frequency estimation of a sinusoidal signal via a three-point interpolated DFT method with high image component interference rejection capability. *Digital Signal Processing*, *24*, 162–169. https://doi.org/10.1016/j.dsp.2013.09.014

[19] Borkowski, J., Mroczka, J., Matusiak, A., & Kania, D. (2021). Frequency Estimation in Interpolated Discrete Fourier Transform with Generalized Maximum Sidelobe Decay Windows for the Control of Power. *IEEE Transactions on Industrial Informatics*, *17*(3), 1614–1624. https://doi.org/10.1109/TII.2020.2998096

[20] Lušin, T., & Agrež, D. (2011). Estimation of the amplitude square using the interpolated discrete Fourier transform. *Metrology and Measurement Systems*, *18*(4), 583–596. https://doi.org/10.2478/v10178-011-0056-6

[21] Borkowski, J., & Kania, D. (2016). Interpolated-DFT-based fast and accurate amplitude and phase estimation for the control of power. *Metrology and Measurement Systems*, *23*(1), 13–26. https://doi.org/10.1515/mms-2016-0013

[22] Shen, T., Li, H., Zhang, Q., & Li, M. (2017). A novel adaptive frequency estimation algorithm based on interpolation FFT and improved adaptive notch filter. *Measurement Science Review*, *17*(1), 48–52. https://doi.org/10.1515/msr-2017-0006

[23] IEEE Std 1057-2017 (Revision of IEEE Std 1057-2007) (2018). IEEE Standard for Digitizing Waveform Recorders. https://doi.org/10.1109/IEEESTD.2018.8291741

[24] Augustyn, J., & Kampik, M. (2019). Improved Sine-Fitting Algorithms for Measurements of Complex Ratio of AC Voltages by Asynchronous Sequential Sampling. *IEEE Transactions on Instrumentation and Measurement*, *68*(6), 1659–1665. https://doi.org/10.1109/TIM.2018.2875901

[25] Aiello, M., Cataliotti, A., & Nuccio, S. (2005). A Chirp-z transform-based synchronizer for power system measurements. *IEEE Transactions on Instrumentation and Measurement*, *54*(3), 1025–1032. https://doi.org/10.1109/TIM.2005.847243

[26] Goertzel, G. (1958). An algorithm for the evaluation of finite trigonometric series. *The American Mathematical Monthly*, 65, 34–35, Mathematical Association of America. https://doi.org/10.2307/2310304

[27] Sysel, P., & Rajmic, P. (2012). Goertzel algorithm generalized to non-integer multiples of fundamental frequency. *EURASIP Journal on Advances in Signal Processing*. https://doi.org/10.1186/1687-6180-2012-56

[28] Kay, S. M. (1993). Fundamentals of statistical signal processing: estimation theory. *Prentice-Hall, Inc*.

[29] IEC 61000-2-2 (2015). Electromagnetic compatibility (EMC) – Part 2–2: Environment – Compatibility levels for low frequency conducted disturbances and signalling in public low-voltage power supply systems, Edition 2.0

**Nuno M. Rodrigues** is enrolled in a Ph.D. program in electrical and computer engineering from Instituto Superior Técnico, University of Lisbon – UL, Lisbon, Portugal. He is researcher of the Instrumentation and Measurement Research Group at the Instituto de Telecomunicações. His current research interests include power quality monitoring and measurements and non-destructive electronic measurement systems.

**Fernando M. Janeiro** received his Licenciatura and Ph.D. degrees in electrical and computer engineering from Instituto Superior Técnico (IST), Technical University of Lisbon (UTL), Lisbon, Portugal, in 1997 and 2004. He is an Assistant Professor with the Department of Mechatronics Engineering from Universidade de Évora, Portugal, where he has been since 2001. He is also a member of the Instrumentation and Measurement Research Group with Instituto de Telecomunicações, where he has been since 1997. His current research interests include power quality measurements, photovoltaic systems, impedance measurements/spectroscopy, and non-destructive testing.

**Pedro M. Ramos** received the Licenciatura, M.Sc. and Ph.D. degrees in electrical and computer engineering from Instituto Superior Técnico, Technical University of Lisbon (now University of Lisbon – UL), Lisbon, Portugal, in 1995, 1997, and 2001. Associate Professor with habilitation from Instituto Superior Técnico, UL and Senior Researcher of the Instrumentation and Measurement Research Group at the Instituto de Telecomunicações. His current research interests include impedance measurements, impedance spectroscopy, sine-fitting algorithms, automatic measurement systems, power-quality monitoring/measurements and non-destructive electronic measurement systems. Member of IMEKO TC4 – Measurement of Electrical Quantities since 2006, Scientific Secretary of IMEKO T4 in 2012-2014 and Vice-Chair of IMEKO TC4 in 2015–2018. IEEE Senior Member since 2013.